Sensors & Actuators: B. Chemical 349 (2021) 130730

Contents lists available at ScienceDirect

Sensors and Actuators: B. Chemical

journal homepage: www.elsevier.com/locate/snb

Carbon nanodot-hybridized silica nanospheres assisted immunoassay for sensitive detection of *Escherichia coli*

Yang Song [a,*], Grayson P. Ostermeyer [b,c], Dan Du [a], Yuehe Lin [a,*]

[a] School of Mechanical and Materials Engineering, Washington State University, Pullman, WA 99164, United States
[b] School of Biological Sciences, Washington State University, Pullman, WA 99164, United States
[c] Outpatient Heart & Vascular/Endoscopy, St. Joseph Regional Medical Center, Lewiston, ID 83501, United States

ARTICLE INFO

Keywords:
Carbon nanodot
Silica nanospheres
ELISA
Immunoassay
High quantum yield
E. coli O157:H7

ABSTRACT

Carbon dots (CDs) are intrinsically luminescent nanomaterials that have many potential applications in biosensing technologies due in part to their high photostability and fluorescent properties. However, attempts to integrate CDs into immunosorbent assays have been deterred by challenges preventing quantum yield augmentation and surface functionalization. To address these issues, we fabricated carbon dot-encapsulated silica nanospheres (CSNs) using a facile one-pot synthesis method. The enclosing silica matrix rendered extensive material stability to the nanospheres and abated quenching by nonradiative decay to cause considerable signal amplification. Nanosphere hybridization to antibodies permitted their use in solid-phase immunoassays as tracers. Here, we demonstrate the suitability of CSN-based immunosorbent assays as a point-of-care technique for the detection of foodborne pathogens through *E. coli* O157:H7 quantitation experiments. After optimization, detection limit of *E. coli* O157:H7 was determined to be 2.4 CFU mL^{-1}. The estimated recoveries were in the range of 91.7–110.5% in spiked samples, which indicated that the developed method is capable for detecting *E. coli* O157:H7 in food samples. The nanosphere tracers described herein, and the methods used to create them, may be beneficial tools for the development of new pathogen biosensing strategies.

1. Introduction

Pathogen surveillance technologies that generate quantitative estimates of microbial contamination are critical tools for preventing disease outbreaks and associated human infections. *E. coli* O157:H7 is a particularly notorious enteric pathogen found in contaminated food and has been implicated in many recent foodborne illness outbreaks [1–7]. The detection of *E.coli* O157:H7 in food samples continues to rely on selective culturing media which need a minimum of 2 days for detection and requires further confirmation tests. Current techniques for detection of multi-pesticides are various, such as solid phase cytometry, viable cell count and fluorescent antibody staining. However, they are limited by technical complexity, sensitivity and cost [57,58]. The harmful nature of these illnesses and the costly healthcare expenses associated with their treatment draw attention to the need to develop new tools dedicated to pathogen monitoring. Sandwich immunoassays (SIAs) are immunodiagnostic techniques that have demonstrated much potential for this purpose [8,9].

Fluorescence-based SIAs have relatively high analytical sensitivities and are capable of detecting large numbers of analytes simultaneously [10–17]. In most SIAs, fluorescent (FL) properties are furnished by molecular chromogens. However, carbon dot (CD) integration offers a new opportunity to improve upon current biosensing standards due to their favorable material qualities, including appreciable solubility in water, cellular biocompatibility, presence of tunable spectral properties [18–28]. Yet, selectively conjugating CDs to biological targets remains a challenge due in part to the nanoscopic dimensions of CDs. The quantity of antibodies that may be grafted to the surfaces of individual CDs is necessarily lower than in larger nanoparticles; so too is the probability of binding antigen. Furthermore, the FL intensity of individual CDs is relatively weak since carbon nanomaterials have characteristically low quantum yields (QYs) [20,29,30]. Calculating the FL intensity of CDs with the goal of engineering CDs with higher quantum yields would be an arduous endeavor, as FL brightness is dependent on complex physicochemical phenomena, including the quantum confinement effect [30,31], conjugated π-domains [32,33], sp^2 carbon networks [34], and variable electronic surface states [35–37]. To improve CD FL brightness, it is necessary to reduce energy quenched through nonradiative decay

* Corresponding authors.
E-mail addresses: yang.song@wsu.edu (Y. Song), yuehe.lin@wsu.edu (Y. Lin).

https://doi.org/10.1016/j.snb.2021.130730
Received 6 July 2021; Received in revised form 31 August 2021; Accepted 7 September 2021
Available online 10 September 2021

and to enhance the rate of radiative decay. Considerable efforts have been made to passivate CDs with the aim of improving FL intensity, as well as to protect CDs from being quenched by exogenous electron donors and acceptors [38,39]. CDs can be relatively complicated to fabricate and purify, which has limited their utilization in conventional bioassays [40]. CD encapsulation is complicated by the tendency of FL nanoparticles to self-aggregate in entrapped states. The surrounding matrix may also sequester some of the radiation from the FL nanoparticle [41]. Developing a facile strategy of CD surface passivation is necessary to enable these nanoparticles to overcome these biosensing hurdles. Recently, a method for coating gold (Au) nanoclusters with silane by silica passivation made FL intensity maintenance possible through a so-called one-pot synthesis strategy. The improvement in observed FL intensity, which occurred without disruption to the Au nanoclusters' stability and tunable surface chemistry, is likely attributable to a reduction in quenching due to nonradiative decay from the Au nanocluster-hybridized silica nanospheres [42].

Here, we use the one-pot synthesis method to fabricate fluorescent CD-hybridized silica nanospheres (CSNs), which we use to detect *E. coli* O157:H7 in vitro as a demonstration of the CSNs' desirable FL and signal amplification properties. The CDs were synthesized from aminosalicylic acid (ASA), a common antibiotic agent, through hydrothermal methods, followed by dialysis membrane purification [55]. The one-pot synthesis process is based on a modified Stöber method, in which as-prepared CDs are co-hydrolyzed with tetraethylorthosilicate (TEOS) in the presence of organic solvent and ammonia [43]. Passivation with silica has various advantages over other polymers or lipids, including a relatively high material stability, an absence of material swelling with pH changes, and easy modification with functional groups. Importantly, silica shells protect the FL intensity of encapsulated CDs. After passivation, silica nanospheres are reacted with the silane coupling substrate, 3-aminopropyltrimethoxysilane (APTES), to introduce amino group for further conjugation. The as-prepared antibody–CSNs serve as novel nanomaterial-labeled probes in SIA systems. Since low infectious doses of *E. coli* O157:H7 contamination can still cause serious illnesses , we selected this pathogen as a model analyte to show the advantages of using CSN tracers compared to other commercially available enzyme-labeled antibodies. Silica nanospheres encapsulated enough CDs to considerably amplify the FL intensity. Furthermore, silica coat encapsulation stabilized FL intensity compared to free CDs. Overall, CSNs possess desirable FL properties that are favorable for pathogen monitoring and may be implemented as a new monitoring tool for preventing foodborne illnesses.

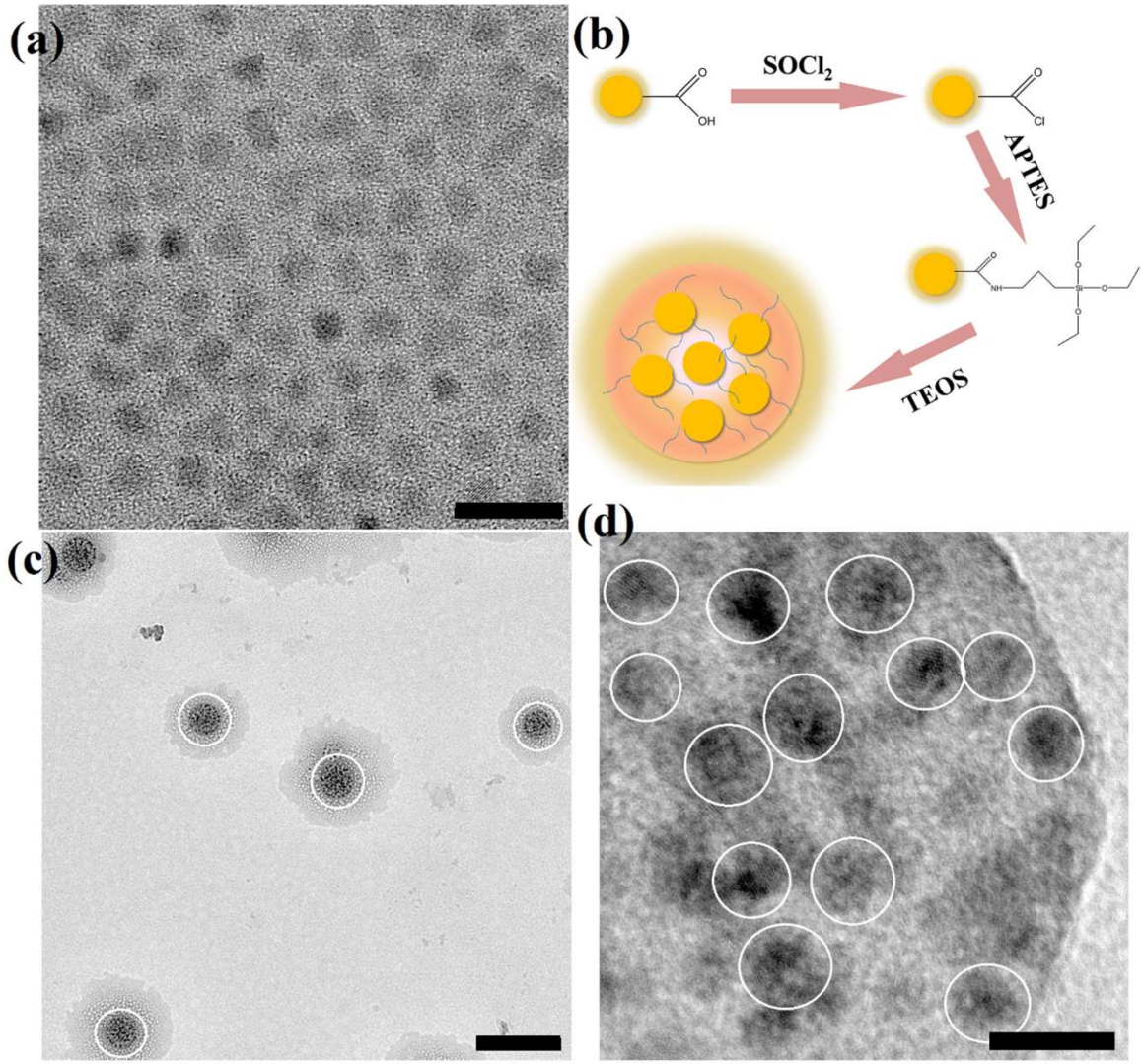

Fig. 1. Fabrication of CDs and CSNs. (a) As-prepared CDs. (b) CSN synthesis scheme. (c) As-prepared CSNs (white circled). (d) HRTEM of a CSN with CDs (white circled) encapsulated by silica. Scale bars: (a) 20 nm, (c) 300 nm, (d) 10 nm.

2. Results and discussion

2.1. Synthesis and characterization of CSNs

CD fabrication begins with the crystallization of ASA in ethanol using a Teflon-lined hydrothermal synthesis autoclave heated to 200 °C for 18 h, followed by tubular membrane dialysis to obtain purified crystals. We evaluated the morphology of as-prepared CDs by transmission electron microscopy (TEM). As shown in Figs. 1a and S1, as-prepared CDs had an average diameter of 6 nm and were spherically shaped. The highly crystalline structure of CDs within individual CSNs was demonstrated by the well-resolved lattice fringes observed using high-resolution TEM (HRTEM), as seen in Fig. 1d. The interplanar distance of the lattice fringes was 0.21 nm, which corresponds to the (001) plane of graphite [44]. The FL emission spectra of CDs and CSNs are overlaid in Fig. 2a. The as-prepared CDs showed relatively rare broad visible range absorption bands, signifying electronic absorption transitions [47]. Excitation with a 365 nm UV laser produced a yellow emission peak at 553 nm [45,46,48]. We estimated the relative QY of UV-excited CDs to be 16.4% based on known luminescence QY data for rhodamine B (Fig. S2).

CSNs were synthesized via copolymerization of CDs and TEOS in alkaline conditions (Fig. 1b). CSNs were monodispersed across micrograph fields of view and had an average particle diameter of 150 nm (Fig. 1c). HRTEM images showed that CDs were randomly distributed within the CSN nanospheres (Fig. 1d). CSNs excited under a 365 nm UV laser produced strong yellow fluorescence and a broad emission spectrum centered at 550 nm (Fig. 2a), which emulates the emission spectrum of excited state CDs. This observation demonstrates that silica nanospheres preserve the spectral properties of CDs. Incidentally, encapsulating silica matrices have been shown to protect organic dyes from self-quenching by operating as 3D spacers which prevent energy transfer between neighboring dyes [54]. Compared with CDs (τ_{ave} = 3.5 ns), the average FL lifetime of CSNs increased to 10.2 ns over time-domain FLIM trials (Fig. 2b), implying a functional advantage of CD encapsulation into silica matrices. In the case of CDs, the fast decay component average was 2.0 ns (76.3%) and the slow decay component was 8.3 ns (23.7%). In the case of CSNs, the fast decay component was lower than that of CDs at 23% (Table S1). Hence, CD encapsulation into silica significantly decreased quenching by nonradiative decay. Importantly, in CSNs the long-lived decay time remained dominant (77%),

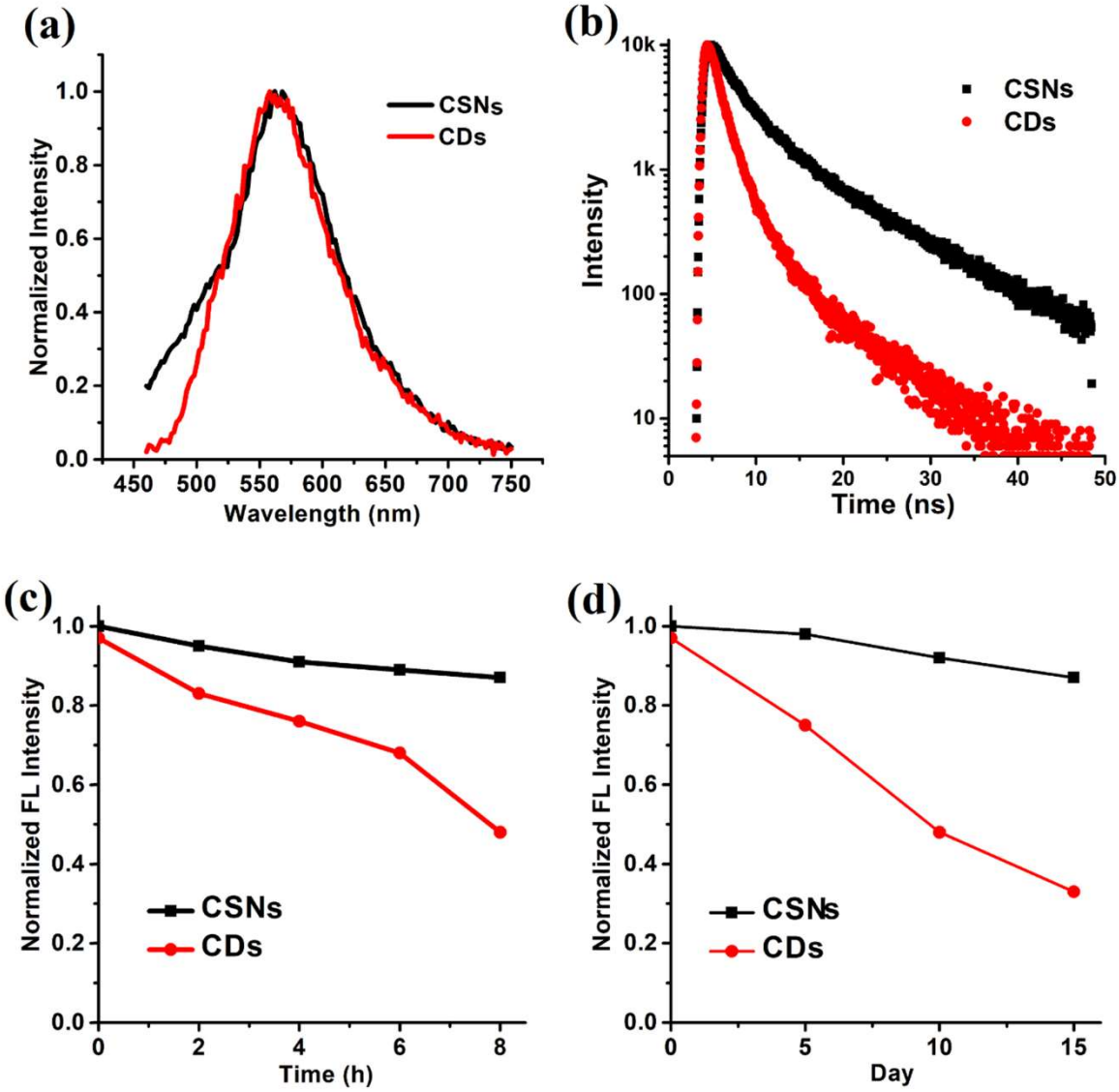

Fig. 2. Fluorescent properties of CDs and CSNs. (a) Normalized fluorescence emission spectra of CSNs and CDs after UV excitation (365 nm). (b) Relative fluorescence lifetime decay curves of CSNs (black) and CDs (red). (c) Fluorescence intensity of CSNs and CDs after intervals of UV irradiation. (d) Fluorescent intensities of CSNs and CDs over 15 days of storage.

supporting the notion that self-quenching by CDs is minimized within the nanospheres. Maintenance of CD fluorescence within the silica nanospheres may be best explained by the cage effect, whereby the encapsulated CDs are confined within the network of silica which effectively suppresses nonradiative decay of the photoexcited state.

To test whether CSNs are suitable as tracers in immunoassay, we investigated several dimensions of CSN stability. Using FL intensity changes to gage the effects of various treatments on CSN stability, we proceeded to test the impact of exposure to ions (PBS), alterations in pH, and UV irradiation, as well as long-term storage of the CSNs. No obvious changes in FL intensity were observed at different ion concentrations in aqueous solutions (Fig. S3), which indicated appropriate material stability for practical applications. Upon UV exposure, the observed FL intensities of CDs continuously decreased, while emission intensity decayed much faster in CDs than in CSNs (Fig. 2c). After 8 h, the effects of photobleaching in CDs were pronounced, as FL intensity had been reduced to 48% of its original value. In contrast, CSNs maintained 88% of their original FL intensity. This result suggests that CSNs harbor more effective anti-photobleaching properties than CDs. We found that CSNs exhibited high chemical and colloidal stability over 15 days of long-term storage (Fig. 2d), which is significant for nanomaterial preservation and transportation. The FL intensity of bare CDs decreased to 39% of its initial value after 15 days of storage in aqueous solution, which contrasted with minimal disturbance in CSN FL performance after storage. Nanomaterials are also vulnerable to sample pH changes. For CDs, the FL intensity decreased at high and low pH values, whereas it remained relatively steady in the pH range from 6 to 11 (Fig. S4). However, CSN FL intensity remained higher and better maintained across a broader range of pH values (4−13). Even at a pH value of 3, CSNs maintained a FL intensity of 41%, indicating that the silica shell may protect the surface state or molecular state of internal CDs from the effects of solvent pH.

2.2. Optimization of the proposed assay

We then employed CSNs as immunoassay tracers to evaluate their performance standards regarding material stability and analytical sensitivity. The nanospheres not only tightly packaged a collection of individually functional CDs into bundles – which in so doing protected the surfaces and molecular states of the internalized CDs from the

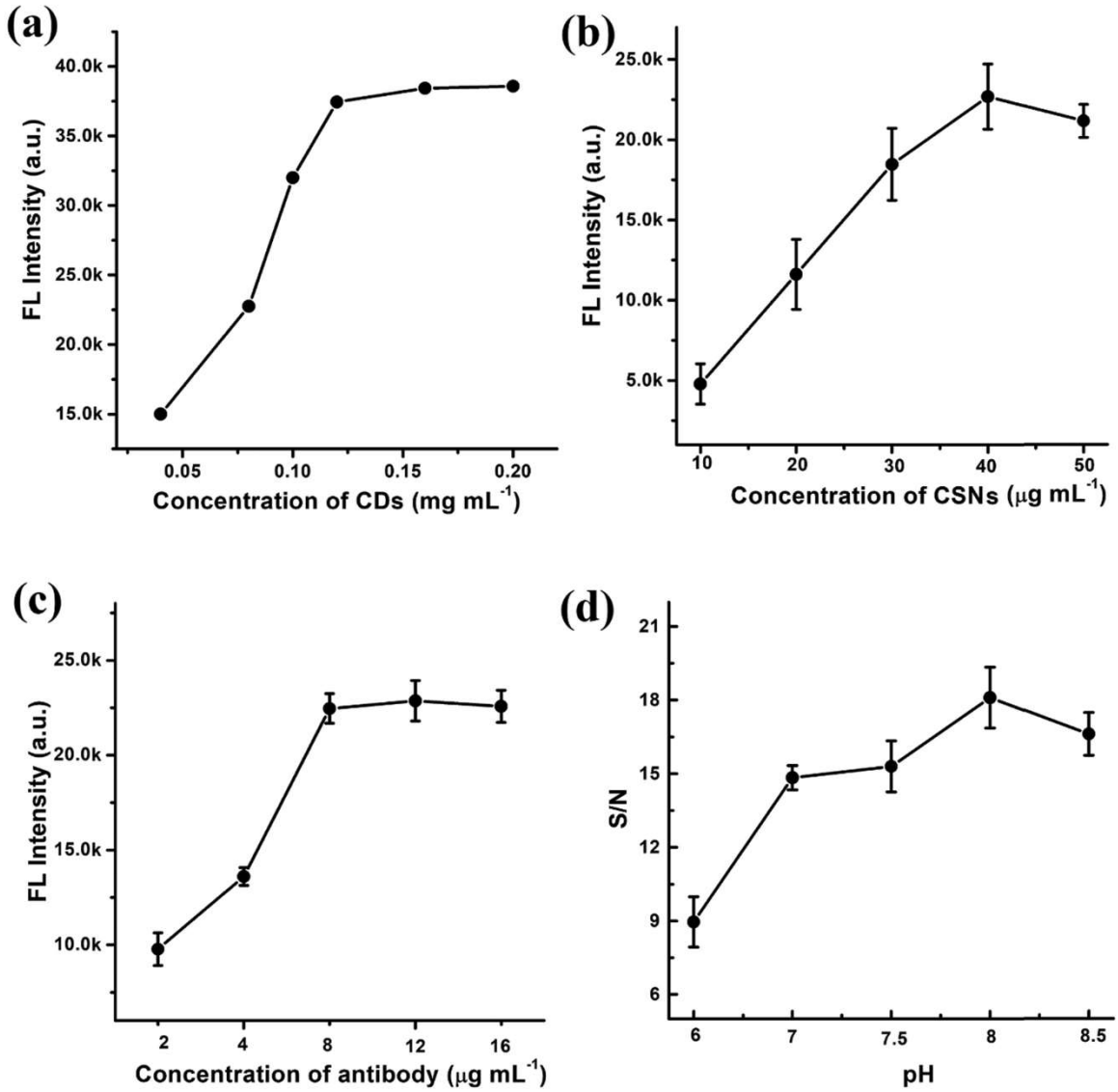

Fig. 3. Optimization of CSN performance standards. (a) Dependence of CSN FL intensity on CD concentration during CSN fabrication. (b) Dependence of CSN FL intensity on CSN concentration mixed with 8 μg mL^{-1} of conjugating antibodies (Ab2); running buffer: PBS (1% BSA). (c) Dependence of FL intensity on Ab2 concentration mixed with 40 μg mL^{-1} of CSNs. (d) Effects of mixture pH on the S/N ratio of ISAs. Bars represent mean standard error.

solvent environment – but they also suppressed nonradiative decay of the CDs' photoexcited states. These features render intrinsic stability and brightness to CSNs. Immunoreaction rate is another performance parameter that is influenced by numerous variables, including the concentration of CDs during CSN synthesis, the concentration of CSNs available during antibody grafting, the frequency of CSN-antibody conjugations, and mixture pH. We observed that as-prepared CSN FL intensity related directly to CD concentration at the time of CSN formation, reaching a plateau at 0.16 mg mL^{-1} (Fig. 3a). A CSN concentration adjusted to 40 μg mL^{-1} prior to antibody conjugation produced optimal FL intensity (Fig. 3b). Moreover, FL intensity related directly to the applied concentration of antibodies up to approximately 12 μg mL^{-1}, suggesting an antibody/CSN ratio most conducive for efficient conjugation (Fig. 3c). We observed that CSN-based ISAs performed optimally at pH 8.0, as revealed by the peak in the signal-to-noise (S/N) ratio (Fig. 3d).

2.3. ISA performance of CSNs

CSNs have unique optical properties and considerable photostability under UV irradiation, suggesting that the nanospheres may be used for biomedical applications, especially ELISA and biosensing platforms. The CSN-based ISA system for quantitative *E. coli* O157:H7 detection is illustrated in Scheme 1. During quantitative ISA experiments, FL intensity increased with increasing *E. coli* O157:H7 concentration (Fig. 4a). The calibration curve between FL intensity and the logarithm of *E. coli* O157:H7 concentration (Fig. 4b) demonstrates the analytical sensitivity of CSN-based ISAs for the analyte concentration range 0–10^4 CFU mL^{-1}, with a correlation coefficient of 0.998 (n = 3). Analyte concentration may be estimated using the equation

$$y = 24712 - \frac{24593}{1 + \sqrt[0.586]{\frac{x}{6378}}}.$$

We calculated the limit of detection (LOD) as 3α/slope, where α represents the standard deviation of the negative control and slope is obtained from the linear calibration plot [56]. We calculated the limit of detection to be 2.4 CFU mL^{-1} (S/N = 3). This finding suggests that the analytical sensitivity of CSN-based ISAs surpasses those reported for other quantitation techniques of *E. coli* O157:H7 concentration (Table 1). Relative to other *E. coli* O157:H7 sensing tools, the limit of detection of CSN-based ISAs is almost 40-fold lower than what is achieved using electrochemical biosensors [49] and nearly 400-fold lower than that of CdSe quantum dot-based immunoassays [50].

To demonstrate the reliability of CSN immunoassays for analyte detection, we calculated the relative standard deviations (RSDs) of observed FL intensity for *E. coli* O157:H7 detection at low (10 CFU mL^{-1}), medium (100 CFU mL^{-1}), and high (1000 CFU mL^{-1}) analyte concentrations. The RSD values were 8.4%, 5.2%, and 6.2%, respectively, indicating satisfactory reproducibility. Another concern related to test fidelity is the potential for nonspecific targeting of antibodies to other pathogens. As described in Fig. 5, we measured the disturbance intensity associated with seven varieties of foodborne pathogen, each present at a concentration of 10^3 CFU mL^{-1}. Only the *E. coli* O157:H7 sample produced strong and significant FL intensity using the same capture antibodies, indicating that the assay components chosen for CSN-based ISAs are associated with high selectivity for *E. coli* O157:H7. The issue of sample colloidal instability obscuring analyte quantitation may persist, but the advantages of this ISA design for pathogen biosensing redress these limitations.

2.4. Trialing mock samples

We then performed recovery studies to interrogate the presence of any interference caused by obstructing agents in the ISA. To do so, we spiked samples of water, milk, and meat juice with three different concentrations of *E. coli* O157:H7 and analyzed the concentrations recovered. The milk and meat juice were diluted 10-fold with 1x PBS to reduce matrix interference. Recovery rates were in the range of 91.7–110.5% (Table 2) and RSD values ranged from 3.1% to 8.1%, which underscored the biosensing accuracy of CSN-based ISAs.

3. Conclusion

In summary, CSNs fabricated using the one-pot method are promising tracer candidates for immunosorbent assay detection of foodborne pathogens. The material properties furnished by silica encapsulation protected internalized CDs and minimized self-quenching by nonradiative decay, thereby augmenting CD fluorescent intensity. We incorporated CSN–antibody conjugates into an immunoassay design to demonstrate their utility in *E. coli* O157:H7 quantitation. CSN-based ISAs exhibited excellent performance in terms of analytical sensitivity and selectivity, and they operated with fidelity under a wide range of

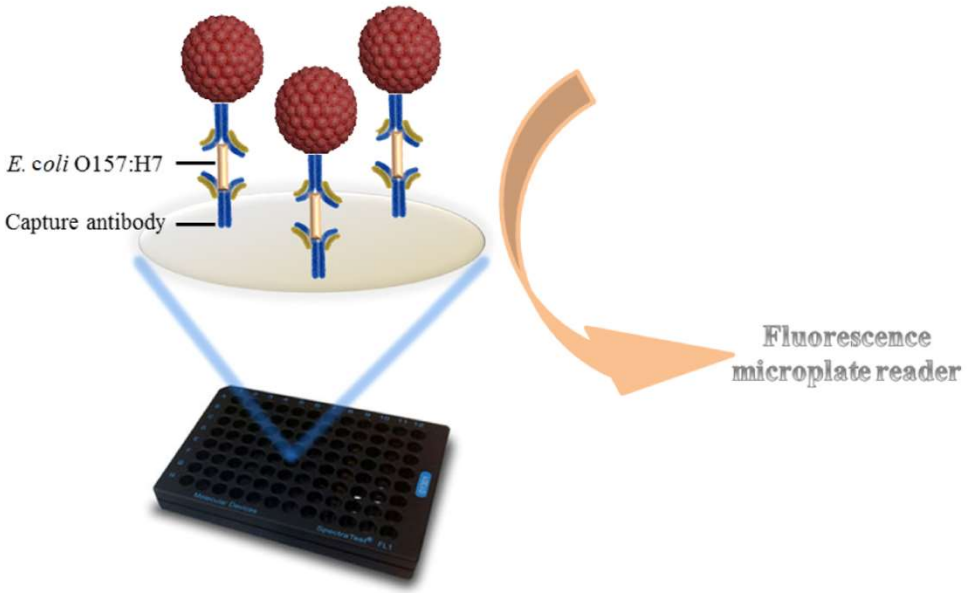

Scheme 1. Illustration of *E. coli* O157:H7 detection using fluorescent CSNs in immunoassay.

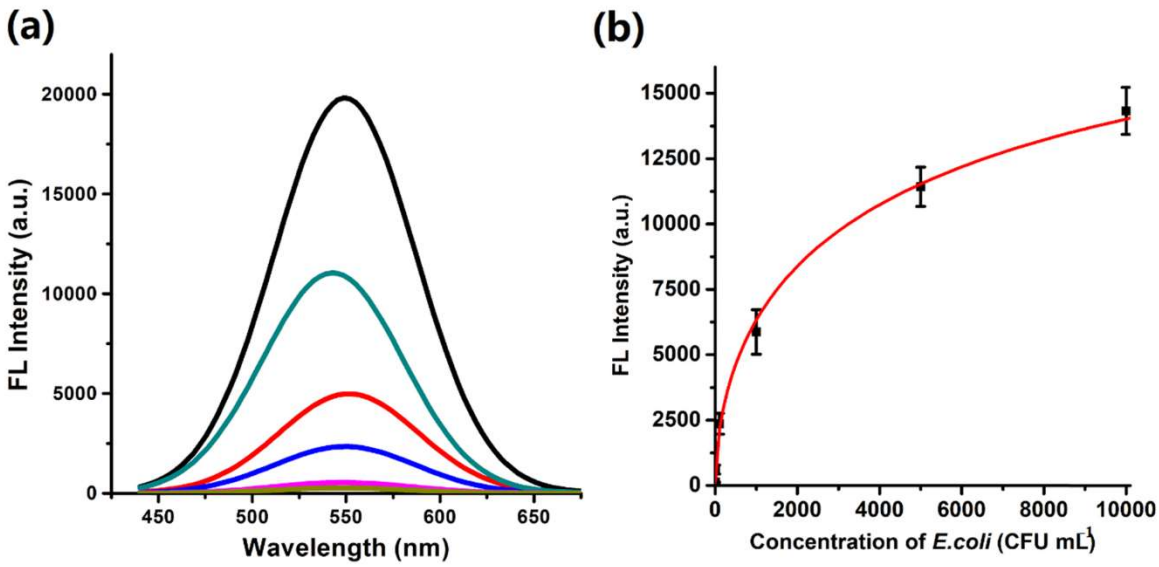

Fig. 4. Calibration of methods for CSN analyte detection. (a) Typical fluorescence response curves of CSN-based ISAs at different *E. coli* O157:H7 concentrations: 0 (beige), 10 (pink), 10^2 (blue), 10^3 (red), 10^4 (teal), and 10^5 CFU mL^{-1} (black). (b) Logistic response of fluorescence intensity to the concentration of *E. coli* O157:H7 in the range 0–10^4 CFU mL^{-1}. Bars represent mean standard error.

Table 1
Comparison of *E. coli* O157:H7 detection methods.

Methods	Detection range (CFU/mL)	LOD (CFU/mL)	Ref.
Electrochemical ELISA	10^3 to 10^8	10^3	[51]
Electrochemical biosensors	10^2 to 10^5	10^2	[49]
ConA-HRP-ELISA	10^2 to 10^5	10^2	[52]
Lateflow immunoassay	10^2 to 10^8	10^2	[53]
CdSe-ELISA	10^3 to 10^7	10^3	[50]
This work	0–10^4	2.4	This work

Table 2
Relative recoveries of *E. coli* O157:H7 from different samples.

Sample	*E. coli* spiked (CFU mL^{-1})	*E. coli* found (CFU mL^{-1})	Recovery (%)	RSD (%)
Water[1]	2.1×10^2	1.926×10^2	91.7	3.1
Water[2]	4.3×10^3	4.08×10^3	94.8	5.0
Milk[1]	2.1×10^2	2.32×10^2	110.5	4.1
Milk[2]	4.3×10^3	4.47×10^3	103.9	5.9
Meat Juice[1]	2.1×10^2	1.86×10^2	93	8.1
Meat Juice[2]	4.3×10^3	3.95×10^2	91.8	6.4

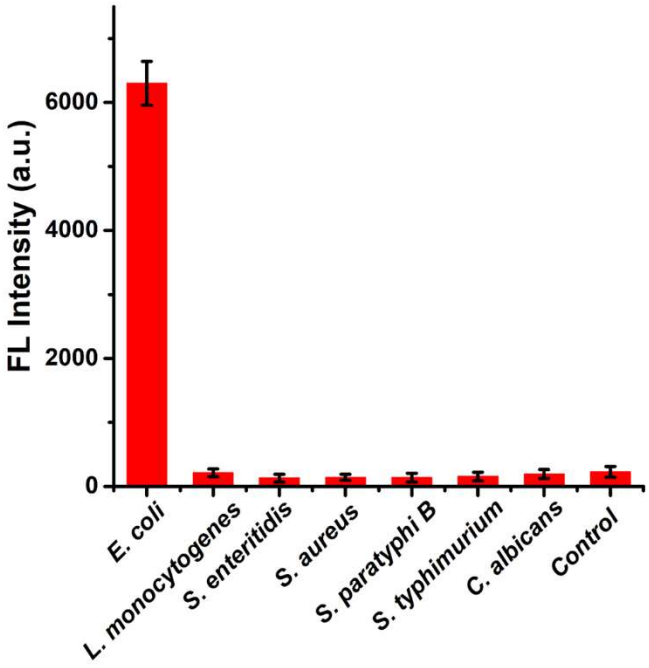

Fig. 5. Specificity of CSN-based ISAs for *E. coli* O157:H7 against seven other types of pathogen (~10^3 CFU/mL). Bars represent mean standard error.

physicochemical conditions. The photostability and high QYs demonstrated by CNSs suggest that they may have other prospective biosensing and bioimaging applications.

4. Experimental section

4.1. Chemicals and materials

Bovine serum albumin (BSA) and 4-aminosalicylic acid were purchased from Sigma-Aldrich. Hydrochloric acid (HCl, 39%) and sodium hydroxide (NaOH) were of analytical grade and purchased from local suppliers. *E. coli* O157:H7 was provided by the School of Food Science at Washington State University. Golt anti-*E. coli* O157:H7 polyclonal antibodies (Ab1, 95058-084) and mouse anti-*E. coli* O157:H7 monoclonal antibodies (Ab2, C507844) were purchased from Kirkegaard & Perry Laboratories, Inc. (Baltimore, Maryland). Millipore ultrapure water was used throughout the experiments.

4.2. Characterization

Transmission electron microscopy (TEM) images were obtained using a Philips CM200 UT (Field Emission Instruments, USA). The tube was operated at a 40 kV accelerating voltage and a 15 mA current. X-ray diffraction (XRD) trials were carried out using a Rigaku Miniflex 600 diffractometer. UV-Vis spectra were obtained using a UV-2450 spectrometer. Dynamic Light Scattering (DLS) measurements were recorded using a Nano ZS analyzer equipped with a solid state He-Ne laser ($\lambda = 633$ nm). Fluorescence spectra were measured with a Cary Eclipse

fluorometer. CD molecular weights were determined using a MALDI-TOF-MS spectrometer (4800 MALDI TOF/TOF Analyzer).

4.3. Synthesis of CDs

Aminosalicylic acid (0.2 g) was dissolved in 20 mL ethanol and then transferred into PTFE autoclaves. After heating the sample at 200 °C for 18 h then cooling the mixture to room temperature, a dark solution was attained. The solution was purified against water using a dialysis bag (MWCO ~ 1.0 kDa) for 1 day to remove small particles. The water was replaced every 6 h. The resultant CDs were freeze dried into a black solid.

4.4. Synthesis of CSNs

A 1:4 ratio (v/v) of CD mixture was obtained by dissolving 4 mg of CDs in 5 mL of $SOCl_2$/acetonitrile. After removing excess $SOCl_2$/acetonitrile by rotary evaporation, COCl–CDs were obtained. The COCl–CD mixture was combined with 2 mL acetonitrile and 50 μL APTES while stirring to produce APTES–CDs (2 mg mL^{-1}). CSNs were synthesized via a modified Stöber method. Briefly, the solution containing 5 mL ethanol and 200 μL of CDs (2 mg mL^{-1}) was stirred and 1 mL ammonia was added. After 10 min of sonication, 200 μL of tetraethylorthosilicate (TEOS) was added under vigorous magnetic stirring. After 12 h of stirring, as-prepared CSNs were washed three times by centrifugation and dissolved in water at a concentration of 1 mg mL^{-1}.

CRediT authorship contribution statement

Y.L. conceived and directed the project. **Y.S.** performed the synthesis and self-assembly of hybrid CSN and did the characterizations and data analysis. **Y.S.** did FRET experiments and analysis and calculated the energy transfer efficacy. **Y.S.** did the immunoassay test for *E. coli* O157:H7 detection. **D.D.** did the data analysis for immunoassay. **Y.S.**, **G.P.O.** and **Y.L.** wrote the manuscript. All authors discussed the results and commented on the manuscript.

Declaration of Competing Interest

The authors declare that they have no known competing financial interests or personal relationships that could have appeared to influence the work reported in this paper.

Acknowledgment

This work was supported by a start-up fund from Washington State University. We are thankful for the staff guidance and facility access at Washington State University's Franceschi Microscopy and Imaging Center, where we acquired our TEM images.

Appendix A. Supporting information

Supplementary data associated with this article can be found in the online version at doi:10.1016/j.snb.2021.130730.

References

[1] J. McCollum, N. Williams, S. Beam, S. Cosgrove, P. Ettestad, T. Ghosh, A. Kimura, L. Nguyen, S. Stroika, R. Vogt, Multistate outbreak of Escherichia coli O157: H7 infections associated with in-store sampling of an aged raw-milk Gouda cheese, 2010, J. Food Prot. 75 (2012) 1759–1765.

[2] K. Nabae, M. Takahashi, T. Wakui, H. Kamiya, K. Nakashima, K. Taniguchi, N. Okabe, A Shiga toxin-producing Escherichia coli O157 outbreak associated with consumption of rice cakes in 2011 in Japan, Epidemiol. Infect. 141 (2013) 1897–1904.

[3] L.W. Riley, R.S. Remis, S.D. Helgerson, H.B. McGee, J.G. Wells, B.R. Davis, R. J. Hebert, E.S. Olcott, L.M. Johnson, N.T. Hargrett, Hemorrhagic colitis associated with a rare Escherichia coli serotype, N. Engl. J. Med 308 (1983) 681–685.

[4] E. Scallan, R.M. Hoekstra, F.J. Angulo, R.V. Tauxe, M. Widdowson, S.L. Roy, J. L. Jones, P.M. Griffin, Foodborne illness acquired in the United States—major pathogens, Emerg. Infect. Dis. 17 (2011) 7–15.

[5] A.M. Wendel, D.H. Johnson, U. Sharapov, J. Grant, J.R. Archer, T. Monson, C. Koschmann, J.P. Davis, Multistate outbreak of Escherichia coli O157:H7 infection associated with consumption of packaged spinach, August-September 2006: the Wisconsin investigation, Clin. Infect. Dis. 48 (2009) 1079–1086.

[6] E.P. Marder, K.N. Garman, L.A. Ingram, J.R. Dunn, Multistate outbreak of Escherichia coli O157: H7 associated with bagged salad, Foodborne Pathog. Dis. 11 (2014) 593–595.

[7] M. Jacob, D. Foster, A. Rogers, C. Balcomb, X. Shi, T. Nagaraja, Evidence of non-O157 shiga toxin–producing Escherichia coli in the feces of meat goats at a US slaughter plant, J. Food Prot. 76 (2013) 1626–1629.

[8] S.M. Schubert, L.M. Arendt, W. Zhou, S. Baig, S.R. Walter, R.J. Buchsbaum, C. Kuperwasser, D.R. Walt, Ultra-sensitive protein detection via Single Molecule Arrays towards early stage cancer monitoring, Sci. Rep. 5 (2015) 11034.

[9] Y. Fan, W. Xiao, Z. Li, X. Li, P.Y. Chuang, B. Jim, W. Zhang, C. Wei, N. Wang, W. Jia, RTN1 mediates progression of kidney disease by inducing ER stress, Nat. Commun. 6 (2015) 7841.

[10] Z. Li, Y. Wang, J. Wang, Z. Tang, J.G. Pounds, Y. Lin, Rapid and sensitive detection of protein biomarker using a portable fluorescence biosensor based on quantum dots and a lateral flow test strip, Anal. Chem. 82 (2010) 7008–7014.

[11] J.V. Jokerst, A. Raamanathan, N. Christodoulides, P.N. Floriano, A.A. Pollard, G. W. Simmons, J. Wong, C. Gage, W.B. Furmaga, S.W. Redding, Nano-bio-chips for high performance multiplexed protein detection: determinations of cancer biomarkers in serum and saliva using quantum dot bioconjugate labels, Biosens. Bioelectron. 24 (2009) 3622–3629.

[12] L. Chen, C. Chen, R. Li, Y. Li, S. Liu, CdTe quantum dot functionalized silica nanosphere labels for ultrasensitive detection of biomarker, Chem. Commun. (2009) 2670–2672.

[13] J. Liu, S.K. Lau, V.A. Varma, B.A. Kairdolf, S. Nie, Multiplexed detection and characterization of rare tumor cells in Hodgkin's lymphoma with multicolor quantum dots, Anal. Chem. 82 (2010) 6237–6243.

[14] D. Lin, J. Wu, F. Yan, S. Deng, H. Ju, Ultrasensitive immunoassay of protein biomarker based on electrochemiluminescent quenching of quantum dots by hemin bio-bar-coded nanoparticle tags, Anal. Chem. 83 (2011) 5214–5221.

[15] U. Resch-Genger, M. Grabolle, S. Cavaliere-Jaricot, R. Nitschke, T. Nann, Quantum dots versus organic dyes as fluorescent labels, Nat. Methods 5 (2008) 763–775.

[16] A. Hoshino, K. Fujioka, T. Oku, M. Suga, Y.F. Sasaki, T. Ohta, M. Yasuhara, K. Suzuki, K. Yamamoto, Physicochemical properties and cellular toxicity of nanocrystal quantum dots depend on their surface modification, Nano Lett. 4 (2004) 2163–2169.

[17] A.M. Derfus, W.C. Chan, S.N. Bhatia, Probing the cytotoxicity of semiconductor quantum dots, Nano Lett. 4 (2004) 11–18.

[18] S.N. Baker, G.A. Baker, Luminescent carbon nanodots: emergent nanolights, Angew. Chem. Int. Ed. 49 (2010) 6726–6744.

[19] L. Cao, M.J. Meziani, S. Sahu, Y. Sun, Photoluminescence properties of graphene versus other carbon nanomaterials, Acc. Chem. Res. 46 (2013) 171–180.

[20] B. Kong, A. Zhu, C. Ding, X. Zhao, B. Li, Y. Tian, Carbon dot-based inorganic-organic nanosystem for two-photon imaging and biosensing of pH variation in living cells and tissues, Adv. Mater. 24 (2012) 5844–5848.

[21] L. Bao, C. Liu, Z. Zhang, D. Pang, Photoluminescence-tunable carbon nanodots: surface-state energy-gap tuning, Adv. Mater. 27 (2015) 1663–1667.

[22] M. Nurunnabi, Z. Khatun, K.M. Huh, S.Y. Park, D.Y. Lee, K.J. Cho, Y. Lee, *In vivo* biodistribution and toxicology of carboxylated graphene quantum dots, ACS Nano 7 (2013) 6858–6867.

[23] X. Li, Y. Liu, X. Song, H. Wang, H. Gu, H. Zeng, Intercrossed carbon nanorings with pure surface states as low-cost and environment-friendly phosphors for white-light-emitting diodes, Angew. Chem. Int. Ed. 54 (2015) 1759–1764.

[24] W. Li, Z. Zhang, B. Kong, S. Feng, J. Wang, L. Wang, J. Yang, F. Zhang, P. Wu, D. Zhao, Simple and green synthesis of nitrogen-doped photoluminescent carbonaceous nanospheres for bioimaging, Angew. Chem. Int. Ed. 52 (2013) 8151–8155.

[25] K. Jiang, S. Sun, L. Zhang, Y. Lu, A. Wu, C. Cai, H. Lin, Red, green, and blue luminescence by carbon dots: full-color emission tuning and multicolor cellular imaging, Angew. Chem. Int. Ed. 54 (2015) 5360–5363.

[26] A. Zhu, Q. Qu, X. Shao, B. Kong, Y. Tian, Carbon-dot-based dual-emission nanohybrid produces a ratiometric fluorescent sensor for in vivo imaging of cellular copper ions, Angew. Chem. Int. Ed. 51 (2012) 7185–7189.

[27] S. Yang, L. Cao, P.G. Luo, F. Lu, X. Wang, H. Wang, M.J. Meziani, Y. Liu, G. Qi, Y. Sun, Carbon dots for optical imaging in vivo, J. Am. Chem. Soc. 131 (2009) 11308–11309.

[28] Y. Li, Y. Hu, Y. Zhao, G. Shi, L. Deng, Y. Hou, L. Qu, An electrochemical avenue to green-luminescent graphene quantum dots as potential electron-acceptors for photovoltaics, Adv. Mater. 23 (2011) 776–780.

[29] Y. Fang, S. Guo, D. Li, C. Zhu, W. Ren, S. Dong, E. Wang, Easy synthesis and imaging applications of cross-linked green fluorescent hollow carbon nanoparticles, ACS Nano 6 (2012) 400–409.

[30] H. Li, X. He, Z. Kang, H. Huang, Y. Liu, J. Liu, S. Lian, C. Tsang, X. Yang, S. Lee, Water-soluble fluorescent carbon quantum dots and photocatalyst design, Angew. Chem. Int. Ed. 49 (2010) 4430–4434.

[31] S. Kim, S.W. Hwang, M. Kim, D.Y. Shin, D.H. Shin, C.O. Kim, S.B. Yang, J.H. Park, E. Hwang, S. Choi, Anomalous behaviors of visible luminescence from graphene quantum dots: interplay between size and shape, ACS Nano 6 (2012) 8203–8208.

[32] Q. Zhao, Z. Zhang, B. Huang, J. Peng, M. Zhang, D. Pang, Facile preparation of low cytotoxicity fluorescent carbon nanocrystals by electrooxidation of graphite, Chem. Commun. (2008) 5116–5118.
[33] B. Qi, H. Hu, L. Bao, Z. Zhang, B. Tang, Y. Peng, B. Wang, D. Pang, An efficient edge-functionalization method to tune the photoluminescence of graphene quantum dots, Nanoscale 7 (2015) 5969–5973.
[34] V. Strauss, J.T. Margraf, C. Dolle, B. Butz, T.J. Nacken, J. Walter, W. Bauer, W. Peukert, E. Spiecker, T. Clark, Carbon nanodots: toward a comprehensive understanding of their photoluminescence, J. Am. Chem. Soc. 136 (2014) 17308–17316.
[35] L. Tang, R. Ji, X. Li, G. Bai, C.P. Liu, J. Hao, J. Lin, H. Jiang, K.S. Teng, Z. Yang, S. P. Lau, Deep ultraviolet to near-infrared emission and photoresponse in layered N-doped graphene quantum dots, ACS Nano 8 (2014) 6312–6320.
[36] A. Mewada, S. Pandey, M. Thakur, D. Jadhav, M. Sharon, Swarming carbon dots for folic acid mediated delivery of doxorubicin and biological imaging, J. Mater. Chem. B 2 (2014) 698–705.
[37] D. Qu, Z. Sun, M. Zheng, J. Li, Y. Zhang, G. Zhang, H. Zhao, X. Liu, Z. Xie, Three colors emission from S, N Co-doped graphene quantum dots for visible light H2 production and bioimaging, Adv. Opt. Mater. 3 (2015) 360–367.
[38] X. Wang, L. Cao, S. Yang, F. Lu, M.J. Meziani, L. Tian, K.W. Sun, M.A. Bloodgood, Y. Sun, Bandgap-Like strong fluorescence in functionalized carbon nanoparticles, Angew. Chem. 122 (2010) 5438–5442.
[39] P. Anilkumar, X. Wang, L. Cao, S. Sahu, J. Liu, P. Wang, K. Korch, K.N. Tackett II, A. Parenzan, Y. Sun, Toward quantitatively fluorescent carbon-based "quantum" dots, Nanoscale 3 (2011) 2023–2027.
[40] X. Wang, L. Cao, F. Lu, M.J. Meziani, H. Li, G. Qi, B. Zhou, B.A. Harruff, F. Kermarrec, Y. Sun, Photoinduced electron transfers with carbon dots, Chem. Commun. (2009) 3774–3776.
[41] X. Liang, X. Li, X. Yue, Z. Dai, Conjugation of porphyrin to nanohybrid cerasomes for photodynamic diagnosis and therapy of cancer, Angew. Chem. 123 (2011) 11826–11831.
[42] P. Huang, J. Lin, S. Wang, Z. Zhou, Z. Li, Z. Wang, C. Zhang, X. Yue, G. Niu, M. Yang, Photosensitizer-conjugated silica-coated gold nanoclusters for fluorescence imaging-guided photodynamic therapy, Biomaterials 34 (2013) 4643–4654.
[43] W. Stöber, A. Fink, E. Bohn, Controlled growth of monodisperse silica spheres in the micron size range, J. Colloid Interface Sci. 26 (1968) 62–69.
[44] L. Tang, R. Ji, X. Cao, J. Lin, H. Jiang, X. Li, K.S. Teng, C.M. Luk, S. Zeng, J. Hao, S. P. Lau, Deep ultraviolet photoluminescence of water-soluble self-passivated graphene quantum dots, ACS Nano 6 (2012) 5102–5110.
[45] R. Liu, D. Wu, S. Liu, K. Koynov, W. Knoll, Q. Li, An aqueous route to multicolor photoluminescent carbon dots using silica spheres as carriers, Angew. Chem. 121 (2009) 4668–4671.
[46] M.J. Krysmann, A. Kelarakis, P. Dallas, E.P. Giannelis, Formation mechanism of carbogenic nanoparticles with dual photoluminescence emission, J. Am. Chem. Soc. 134 (2012) 747–750.
[47] Pan, L. Sun, S., Zhang, A., Jiang, K., Zhang, L., Dong, C., Huang, Q., Wu, A., Lin, H., Truly fluorescent excitation-dependent carbon dots and their applications in multicolor cellular imaging and multidimensional sensing. Adv. Mater. 2015, n/a-n/a.
[48] J. Shang, L. Ma, J. Li, W. Ai, T. Yu, G.G. Gurzadyan, The origin of fluorescence from graphene oxide, Sci. Rep. 2 (2012) 792.
[49] A.H.A. Hassan, A. de la Escosura-Muñiz, A. Merkoçi, Highly sensitive and rapid determination of Escherichia coli O157: H7 in minced beef and water using electrocatalytic gold nanoparticle tags, Biosens. Bioelectron. 67 (2015) 511–515.
[50] L. Yang, Y. Li, Simultaneous detection of Escherichia coli O157: H7 and Salmonella Typhimurium using quantum dots as fluorescence labels, Analyst 131 (2006) 394–401.
[51] M.R. Akanda, V. Tamilavan, S. Park, K. Jo, M.H. Hyun, H. Yang, Hydroquinone diphosphate as a phosphatase substrate in enzymatic amplification combined with electrochemical–chemical–chemical redox cycling for the detection of E. coli O157: H7, Anal. Chem. 85 (2013) 1631–1636.
[52] H. Zhang, Y. Shi, F. Lan, Y. Pan, Y. Lin, J. Lv, Z. Zhu, Q. Jiang, C. Yi, Detection of single-digit foodborne pathogens with the naked eye using carbon nanotube-based multiple cycle signal amplification, Chem. Commun. 50 (2014) 1848–1850.
[53] T. Jiang, Y. Song, T. Wei, H. Li, D. Du, M. Zhu, Y. Lin, Sensitive detection of Escherichia coli O157: H7 using Pt–Au bimetal nanoparticles with peroxidase-like amplification, Biosens. Bioelectron. 77 (2016) 687–694.
[54] X. Zhao, R.J. Bagwe, W. Tan, Development of organic-dye-doped silica nanoparticles in a reverse microemulsion, Adv. Mater. 16 (2004) 173–176.
[55] Y. Song, C. Zhu, J. Song, H. Li, D. Du, Y. Lin, Drug-derived bright and color-tunable N-doped carbon dots for cell imaging and sensitive detection of Fe3+ in living cells, ACS Appl. Mater. Interfaces 9 (8) (2017) 7399–7405.
[56] N. Cheng, Y. Song, Q. Fu, D. Du, Y. Luo, Y. Wang, W. Xu, Y. Lin, Aptasensor based on fluorophore-quencher nano-pair and smartphone spectrum reader for on-site quantification of multi-pesticides, Biosens. Bioelectron. 117 (2018) 75–83.
[57] J. Baudart, P. Lebaron, Rapid detection of Escherichia coli in waters using fluorescent in situ hybridization, direct viable counting and solid phase cytometry, J. Appl. Microbiol. 109 (4) (2010) 1253–1264.
[58] N. Yamaguchi, M. Sasada, M. Yamanaka, M. Nasu, Rapid detection of respiring Escherichia coli O157:H7 in apple juice, milk, and ground beef by flow cytometry, Cytom. Part A: J. Int. Soc. Anal. Cytol. 54 (1) (2003) 27–35.

Yang Song is Scientist of Nanosong System LLC. He puts his interests on the development of nanozymes for environmental analysis and biochemical sensing.

Grayson P. Ostermeyer is a master student of Washington State University. He focuses on new enzyme mimics and their promising use in biological detection.

Dan Du obtained her Ph.D. from Nanjing University, and now is a professor of Washington State University. Her research interests focus on functional nanomaterials for sensing. She has published more than 300 papers with an H-index of 70.

Yuehe Lin is a professor of Washington State University. His research interests focus on chemical sensors/biosensors, electrochemistry, and nanomaterial synthesis and their emerging applications. He has published more than 500 papers with an H-index of 110. He is a fellow of NAI, WSAS, AAAS, RSC, and AIMBE.